# Nonlinear Science

#### RESEARCH



# Curvature Driven Complexity in the Defocusing Parametric Nonlinear Schrödinger System

Keith Promislow<sup>1</sup> • Abba Ramadan<sup>2</sup>

Received: 21 August 2023 / Accepted: 19 January 2024 © The Author(s), under exclusive licence to Springer Science+Business Media, LLC, part of Springer Nature 2024

#### **Abstract**

The parametric nonlinear Schrödinger equation models a variety of parametrically forced and damped dispersive waves. For the defocusing regime, we derive a normal velocity for the evolution of curved dark-soliton fronts that represent a  $\pi$ -phase shift across a thin interface. We establish a simple mechanism through which the parametric term transitions the normal velocity evolution from a curvature-driven flow to motion against curvature regularized by surface diffusion of curvature. In the former case interfacial length shrinks, while in the latter case interface length generically grows until self-intersection followed by a transition to complex motion.

**Keywords** Curve lengthening  $\cdot$  Surface diffusion  $\cdot$  Normal velocity  $\cdot$  Curvature driven flow  $\cdot$  Parametric nonlinear Schrödinger equation

**Mathematics Subject Classification** 35C20 · 35P15

#### 1 Introduction

The parametric nonlinear Schrödinger (PNLS) equation is a general model for parametrically forced surface waves and for pattern formation. It has been derived in the context of Faraday waves (Zhang and Viñals 1995) where increased driving force drives transitions to zigzag patterns and complex behavior. The PNLS has also been derived as a model of phase sensitive amplifiers (Alexander et al. 1997) and in the

Communicated by Peter Miller.

promislo@msu.edu

Published online: 28 February 2024

Department of Mathematics, Michigan State University, East Lansing, MI 48824, USA

Department of Mathematics, The University of Alabama, Tuscaloosa, AL 35401, USA



40 Page 2 of 20 Journal of Nonlinear Science (2024) 34:40

large detuning limit of optical parametric oscillator systems (Coulibaly et al. 2008; Izús et al. 1999; Promislow and Kutz 2000; Taki et al. 2000; Trillo et al. 1997). More recently it has been proposed as a model for dissipative self organization (Ropp et al. 2018) and as a template for second-order phase transitions between degenerate and non-degenerate regimes (Roy et al. 2021), Coulibaly et al., (2014).

We present an analysis of the evolution of curved dark-soliton fronts in the 1+2D PNLS equation. These fronts represent  $\pi$ -phase shifts in the optical field. We consider interfaces that have bounded curvatures and derive a normal velocity that describes the temporal evolution of the front. In particular if the parametric strength decreases through a critical value the normal velocity transitions from a curvature-driven flow to motion *against* curvature regularized by surface diffusion of curvature. Specifically in the limit in which the ratio of dispersive length scale to domain size is small ( $\epsilon \ll 1$ ) we identify a bifurcation parameter  $\mu$  for which the normal velocity V of the dark-soliton interface admits the expansion

$$V = -\alpha \kappa_0 + \epsilon^2 (\nu \Delta_s \kappa_0 + \zeta \kappa_0^3) + O(\epsilon^4). \tag{1}$$

Here  $\kappa_0$  is the curvature of the interface,  $\Delta_s$  is the Laplace-Beltrami surface diffusion operator, and  $\alpha$ ,  $\nu$  and  $\zeta$  are  $\mu$ -dependent real coefficients. The leading order coefficient  $\alpha$  has the same sign as  $\mu$ , its sign change encodes the transition between motion with and against curvature. Crucially we establish the existence of  $\mu_* > 0$ , independent of  $\epsilon$ , such that  $\nu > 0$  if  $|\mu| < \mu_*$ . This allows the surface diffusion to regularize the motion against curvature that arises for  $\mu$  < 0. Moreover the transition flips the system from one in which interface length shortens suggesting a convergence to equilibrium, to one in which interface length grows without bound, with meandering evolution that generically leads to self-intersection. Indeed numerical observations provided in Section 4 show that after self-intersection the dark fronts form cells that engage in a complex jostling motion. Such curvature flow transitions have been studied in dissipative systems such as polymer melts, Chen and Promislow (2023) but their presence in a dispersive system are here-to-fore unstudied. The analysis presented here is formal but is complemented with a sharp characterization of the transverse spectrum of the wave which shows that the curvature transition is not associated with any transverse instability of the dark soliton.

The paper is organized as follows. In Sect. 2 the PNLS system and the analysis of the 1D transfer spectral problem are presented. In Sect. 3 the inner and outer asymptotic formulations of the system are developed and normal velocity is resolved. Section 4 presents consequences of the bifurcation in the normal velocity and outlines the impact on simulations of the full system.

# 2 PNLS and One-Dimensional Spectral Analysis

The PNLS system describes the evolution of a complex phase  $\Theta \in H^2(\Omega)$ ,

$$i\Theta_t + \frac{\epsilon^2}{2}\Delta\Theta - |\Theta|^2\Theta + (i+a)\Theta - \gamma\Theta^* = 0, \tag{2}$$



on a spatially periodic domain  $\Omega = [0, L]^2$ . Here  $0 < \epsilon \ll 1$  is a small parameter that characterizes the ratio of the dispersive lengthscale to domain size, a is a phase rotation and  $\gamma$  is the parametric pump strength. We rescale the complex phase  $\Theta$ , time t

$$\Theta = \frac{2}{\sqrt{\beta}} u(\tilde{x}) e^{i\theta},$$

$$\tau = 2t/\beta,$$
(3)

and space  $\tilde{x} = 2x/\sqrt{\beta}$  where

$$\beta := \frac{4}{a + \sqrt{\gamma^2 - 1}} > 0,$$

and the phase angle  $\theta$  as the solution of

$$\gamma e^{-2i\theta} = -\sqrt{\gamma^2 - 1} + i.$$

We drop the tilde's and introduce the real vector function  $U = (\Re u, \Im u)^t$  which satisfies

$$U_{\tau} = F(U) := \begin{pmatrix} 0 & -(\epsilon^2 \Delta - 2|U|^2 + 1 - \mu) \\ (\epsilon^2 \Delta - 2|U|^2 + 2) & -\beta \end{pmatrix} U, \quad (4)$$

where the bifurcation parameter

$$\mu := -\frac{a - 3\sqrt{\gamma^2 - 1}}{a + \sqrt{\gamma^2 - 1}},$$

lies in [-1, 3]. In what follows, a shift from  $\mu > 0$  to  $\mu < 0$  will trigger the transition in curvature motion.

Posed on the line  $\mathbb{R}$ , in the scaled coordinate  $z = x/\epsilon$ , and the PNLS system has a dark-soliton steady-state solution

$$\Phi_0(z) = \begin{pmatrix} \phi(z) \\ 0 \end{pmatrix},\tag{5}$$

where  $\phi(z) = \tanh(z)$ , solves

$$\partial_z^2 \phi - 2\phi^3 + 2\phi = 0. ag{6}$$

The linearization of the 1D PNLS system about  $\Phi_0$  yields the system

$$W_{\tau} = LW, \tag{7}$$

40 Page 4 of 20 Journal of Nonlinear Science (2024) 34:40

where the 1D linear operator L is given by

$$L = \begin{pmatrix} 0 & D \\ -C & -\beta \end{pmatrix}, \tag{8}$$

with

$$C = -\partial_z^2 - 6\psi^2 + 4,D = -\partial_z^2 - 2\psi^2 + \mu + 1,$$
(9)

and  $\psi(x) = \operatorname{sech}(x)$ . These operators have point spectrum-eigenfunction pairs

$$\sigma_p(C) = \{(0, \phi'), (3, \phi \psi)\}, 
\sigma_p(D) = \{(\mu, \psi)\}.$$
(10)

The operators C and D may have other point spectrum in their respective gaps (3, 4) and  $(\mu, 1 + \mu)$  between their largest point spectrum and the branch point of their essential spectrum. The characterization of these ground state eigenvalues and the essential spectrum show that  $C \ge 0$  and D > 0 if  $\mu > 0$ , while the dimension n(D) of the negative space of D satisfies  $n(D) \ge 1$  if  $\mu < 0$ . A structural point of the analysis arises from the generic fact that that ground states of the Sturmian operators C and D are both nonzero with full support, and hence can not be orthogonal.

# 2.1 Essential Spectrum of L

To characterize the essential spectrum of L substitute  $W = e^{\lambda \tau} e^{isx} V$  into (7) to obtain an eigenvalue problem for V,

$$\lambda V = \begin{pmatrix} 0 & s^2 + 2(1+\mu) \\ -s^2 - 4 & -\beta \end{pmatrix} V, \tag{11}$$

which has nontrivial solutions for

$$\lambda = \frac{-\beta \pm \sqrt{\beta^2 - 4(s^2 + 1 + \mu)(s^2 + 4)}}{2}.$$
 (12)

The maximum of  $\Re \lambda$  occurs at s=0, and hence all  $\lambda \in \sigma_{ess}(L)$  satisfy

$$\Re \lambda \le \lambda_M := \Re \left( \frac{-\beta + \sqrt{\beta^2 - 16(1 + \mu)}}{2} \right) < 0. \tag{13}$$

### 2.2 The Kernel of L

The operator C has a kernel and from Lemma 3.5 of Promislow and Kutz (2000) we know that  $\lambda = 0$  is a simple eigenvalue of L, for all  $\mu$ . For  $\mu \neq 0$  the kernel of L and



40

of its adjoint L<sup>†</sup> are spanned by the vectors

(2024) 34:40

$$\Psi_0 = \begin{pmatrix} \phi' \\ 0 \end{pmatrix}, \qquad \Psi_0^{\dagger} = \begin{pmatrix} \beta D^{-1} \phi' \\ \phi' \end{pmatrix} \tag{14}$$

, respectively. Here and below † denotes the operators and associated eigenvectors associated to the adjoint with respect to the  $L^2(\Omega)$  inner product. For  $\mu = 0$  the kernels remain simple and are spanned by

$$\Psi_0 = \begin{pmatrix} \phi' \\ 0 \end{pmatrix}, \quad \Psi_0^{\dagger} = \begin{pmatrix} \psi \\ 0 \end{pmatrix}.$$
(15)

When scaled to have unit norm, the eigenfunctions are smooth functions of  $\mu$ .

The inverse of L is given by

$$L^{-1} = \begin{pmatrix} -\beta C^{-1} D^{-1} & -C^{-1} \\ D^{-1} & 0 \end{pmatrix}.$$
 (16)

When C and D have kernels attention is required to insure that the inverses act on their domain.

# 2.3 Point Spectrum of L

Theorem 3.6 of Promislow and Kutz (2000) establishes the existence of  $\lambda_M > 0$  such that

$$\sigma(L) \subset \{\lambda | \Re \lambda < -\lambda_M\} \cup \{0\}.$$

We provide an alternate proof that generalizes more readily from operators that act on  $H^2(\mathbb{R})$  to operators that act on the multidimensional space  $H^2(\Omega)$ . The  $L^2$  inner product and norm on  $\mathbb{R}$  are denoted  $\langle f, g \rangle$  and || f || for  $f, g : \mathbb{R} \mapsto \mathbb{R}^n$  for  $n \geq 1$ .

The point spectrum of L is comprised of eigenfunctions localized in x that solve

$$\lambda P = \begin{pmatrix} 0 & D \\ -C & -\beta \end{pmatrix} P. \tag{17}$$

As two equations for the two unknowns  $P = (P_1, P_2)^t$  satisfies

$$\lambda P_1 = DP_2, (\lambda + \beta)P_2 = -CP_1.$$
 (18)

Assuming that  $\lambda \neq 0$  then  $P \perp \Psi_0^{\dagger}$ . For  $\mu \neq 0$  we combine this with the first equation of (14) and deduce that either  $\lambda = -\beta < 0$  or

$$P_1 \perp D^{-1} \phi'$$
 and  $P_2 \perp \phi'$ .

For  $\mu \neq 0$  the operator D > 0 is invertible and we may solve for  $P_1$ ,

$$CP_1 + \lambda(\lambda + \beta)D^{-1}P_1 = 0.$$

Taking the complex-valued inner product with  $P_1$  yields the relation

$$\lambda(\lambda + \beta) = -\frac{\langle CP_1, P_1 \rangle}{\langle D^{-1}P_1, P_1 \rangle} =: \rho_1.$$
 (19)

The quadratic formula shows that

$$\lambda = \frac{-\beta \pm \sqrt{\beta^2 - 4\rho_1}}{2}.\tag{20}$$

In particular we deduce that  $\sigma_p(L)$  resides in the range of the right-hand side over the possible values of  $\rho_1$ . In particular if  $\rho_1 > 0$  then  $\Re \lambda < -\rho_1/\beta < 0$ . For  $\mu \neq 0$  this motivates the definition of  $X_*(\mu) = \{D^{-1}\phi'\}^{\perp}$  and the real number,

$$\rho_*(\mu) := \min_{P_1 \in X_*} \frac{\langle CP_1, P_1 \rangle}{\langle D^{-1}P_1, P_1 \rangle}.$$
 (21)

**Lemma 1** There exists  $\mu_*, d_+ > 0$  such that  $D|_{X_*} > d_+$  for all  $\mu \in [-\mu_*, 3]$ .

**Proof** We apply Proposition 5.3.1 of Kapitula and Promislow (2013), see also Kapitula and Promislow (2012), to the operator D constrained to act on  $X_*$ . Taking  $\mu_* < 0$  with  $|\mu_*|$  sufficiently small, then D has negative index  $n(D) \le 1$  for all  $\mu \in [-\mu_*, 3]$ . We deduce that

$$n\left(D\big|_{X_*}\right) = n(D) - n(A),\tag{22}$$

where  $A = \langle D^{-1}(D^{-1}\phi'), D^{-1}\phi' \rangle \in \mathbb{R}$ . Recalling that  $\psi$  is the ground state of D with eigenvalue  $\mu$ , we write

$$\phi' = \frac{\langle \phi', \psi \rangle}{\|\phi'\| \|\psi\|} \psi + \psi^{\perp}, \tag{23}$$

where  $\psi^{\perp} \in X_D := \{\psi\}^{\perp}$  satisfies  $\|\psi^{\perp}\| \leq \|\phi'\|$ . In particular we have the relation

$$D^{-3}\phi' = \frac{\langle \phi', \psi \rangle}{\|\phi'\| \|\psi\|} \frac{\psi}{\mu^3} + D^{-3}\psi^{\perp}.$$

Since  $X_D$  is a spectral subspace of D it follows that  $\sigma\left(D\big|_{X_D}\right) = \sigma(D)\setminus\{\mu\}$ . Hence there exists  $\mu_*>0$  and a constant  $\tilde{d}_+>0$  such that  $D\big|_{X_D}\geq \tilde{d}_+$  for  $\mu\in[-\mu_*,3]$ . We deduce that

$$\left| A - \frac{|\langle \phi', \psi \rangle|^2}{\|\phi'\| \|\psi\|} \frac{1}{\mu^3} \right| \le \tilde{d}_+^{-3} \|\phi'\|^2.$$



It follows that A<0 if  $\mu\in[-\mu_*,0)$  for  $\mu_*>0$  sufficiently small. Moreover we have the limit  $A\to-\infty$  at  $\mu\to0^-$ . The index relation (22) implies that  $n\left(D\big|_{X_*}\right)=0$  for  $\mu\in(-\mu_*,0]$ . Since D>0 for  $\mu>0$ , the negative index of D is zero for  $\mu\in[-\mu_*,3]$ . The lower bound of  $D\big|_{X_*}$  is given by its ground state eigenvalue. The ground state eigenvalue is continuous in  $\mu$ , and the existence of  $d_+>0$  follows.  $\square$ 

**Proposition 2** There exists  $\mu_* > 0$  such that  $\rho_*(\mu) > 0$  for  $\mu \in [-\mu_*, 3]$ .

**Proof** The operator C has a simple kernel spanned by  $\phi'$  and is strictly positive on  $\{\phi'\}^{\perp}$ . The operator  $C|_{X_{\perp}}$  is strictly positive as long as

$$\langle D^{-1}\phi', \phi' \rangle \neq 0.$$

This is obvious for  $\mu > 0$  since D is positive there. For  $\mu < 0$  we use the decomposition (23) to write

$$\left| \langle \mathbf{D}^{-1} \phi', \phi' \rangle - \frac{\langle \phi', \psi \rangle^2}{\|\phi'\| \|\psi\|} \frac{1}{\mu} \right| \le \tilde{d}_+ \|\phi'\|^2. \tag{24}$$

This implies the existence of  $\mu_* > 0$  for which the inner product is not zero for all  $\mu \in [-\mu_*, 3]$ . That is there exists a constant  $c_+ > 0$  such that  $C\big|_{X_*} \ge c_+$  for all values of  $\mu \in [-\mu_*, 3]$ . For these  $\mu$  we deduce that for all  $P_1 \in X_*$ 

$$\langle CP_1, P_1 \rangle \ge c_+ ||P_1||^2,$$
  
 $\langle D^{-1}P_1, P_1 \rangle \le d_+^{-1} ||P_1||^2.$ 

It follows that  $\rho_* > c_+ d_+ > 0$  for these  $\mu$ .

**Theorem 3** There exists  $\mu_*$ ,  $\lambda_M > 0$  such that for all  $\mu \in [-\mu_*, 3]$  the spectrum of L satisfies

$$\sigma(L) \subset \{0\} \cup \{\Re \lambda < -\lambda_M\}. \tag{25}$$

*Moreover the kernel of* L *is simple.* 

**Proof** The essential spectrum of L lies strictly in the left-half complex plane. If  $\lambda \in \sigma_p(L) \setminus \{0\}$ , then the relation (20) holds with  $\rho_1$  as defined in (19). By definition of  $\rho_*$  we have  $\rho_1 > \rho_* > 0$ . From the Taylor expansion of the right-hand side of (20)

$$\Re \lambda < -\frac{\rho_*}{\beta}.$$

Defining  $\lambda_M = \rho_*/\beta$  completes the proof.

#### 3 Curvature Driven Flow

We consider a smooth, closed interface  $\Gamma = \{ \gamma(s) \mid s \in [0, L] \}$  that breaks  $\Omega$  into two regions  $\{ \Omega_+, \Omega_- \}$  and introduce the local Frenet coordinates

$$x = \gamma(s) + n(s)z/\epsilon, \tag{26}$$

40 Page 8 of 20 Journal of Nonlinear Science (2024) 34:40

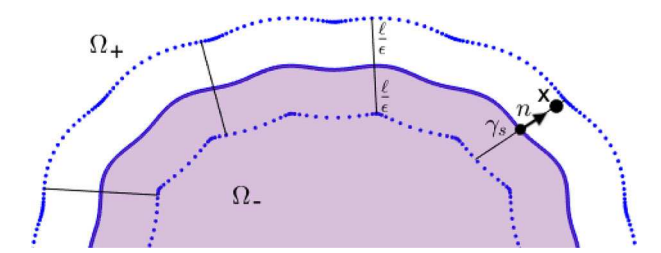


Fig. 1 Sketch of the Frenet coordinates associated to curve  $\gamma$  (indicated by solid line) and the neighborhood  $|z| < \ell/\epsilon$  bounded by the dotted lines. The region  $\Omega_+$ , containing the set z > 0, is unshaded and  $\Omega_-$ , containing the set z < 0, is shaded. Four normal lines are sketched, and the decomposition (26) of a generic point x within the neighborhood into a base point  $\gamma_s = \gamma(s)$  and distance z along the normal n = n(s) is illustrated

where n(s) is the unit outward normal to the curve  $\Gamma$  at point  $\gamma(s)$  and z is signed,  $\epsilon$ -scaled distance to  $\Gamma$ , see Fig. 1. If the interface  $\gamma$  has smooth, bounded curvatures and is far from self-intersection then the change of variables from  $x=(x_1,x_2)$  to (s,z) is well defined on a neighborhood of  $\Gamma$ . Indeed there exists  $\ell>0$  such that the neighborhood contains all points  $x\in\Omega$  for which the scaled distance to  $\Gamma$  satisfies  $z(x)<\ell/\epsilon$ . We introduce  $\overline{\phi}$  which is a smooth function that agrees with  $\phi$  for  $|z|<\ell/(2\epsilon)$  and is identically 1 for  $z>\ell/\epsilon$  and identically -1 for  $z<-\ell/\epsilon$ . The truncated function  $\overline{\phi}$  induces a smooth function  $\Phi$  defined on  $\Omega$ ,

$$\Phi(x) := \begin{pmatrix} \overline{\phi}(z(x)) \\ 0 \end{pmatrix} \quad |z| < \ell/\epsilon, \tag{27}$$

and  $\Phi(x) = \pm 1$  if  $z > \ell/\epsilon$  or  $z < -\ell/\epsilon$  respectively. Since  $\phi$  decays exponentially to the constant values  $\pm 1$  at an O(1) rate in z, this modification induces exponentially small perturbations that do not impact the analysis. The overbar on  $\phi$  is dropped in the sequel. The evolution of U is tracked via its interface map  $\gamma = \gamma(s, \tau)$  whose motion is prescribed by the normal velocity which controls the evolution of the curvature through the relation (49) given below. Knowledge of the curvatures is equivalent to prescribing  $\gamma$  up to rigid body motion.

# 3.1 Outer Expansion

The outer region is divided into inside z < 0 and outside z > 0 sets,  $\Omega_{\pm}$ . These regions are described by Cartesian variables. We expand the ansatz as

$$U = \begin{pmatrix} p \\ q \end{pmatrix} = u_0 + \epsilon u_1 + \epsilon^2 u_2 + O(\epsilon^3),$$

where each term has a vector decomposition

$$u_i = \begin{pmatrix} p_i \\ q_i \end{pmatrix}, \qquad i = 0, 1, 2, \dots$$



To match with the ansatz (27) we impose

$$u_0 = \begin{pmatrix} p_0 \\ q_0 \end{pmatrix} = \begin{pmatrix} \mathbb{I}_{\Omega_+} - \mathbb{I}_{\Omega_-} \\ 0 \end{pmatrix},$$

where  $\mathbb{I}_E$  denotes the indicator function of the set E. This yields an expansion of the residual F(U) in the form

$$F(U) = \begin{pmatrix} 0 \\ 2(1 - p_0^2)p_0 \end{pmatrix} + \epsilon \begin{pmatrix} (2p_0^2 - 1 - \epsilon)q_1 \\ -\beta q_1 - 4p_0^2p_1 \end{pmatrix} + \epsilon^2 \begin{pmatrix} (2p_0^2 - 1 - \epsilon)q_2 + 4p_0p_1q_1 \\ -\beta q_2 - 4p_0p_1^2 + L_2p_0 \end{pmatrix} + O(\epsilon^3).$$
 (28)

Since  $p_0^2 = 1$  in both domains this affords the reduction

$$F(U) = \epsilon \begin{pmatrix} (1+\mu)q_1 \\ -\beta q_1 - 4p_1 \end{pmatrix} + \epsilon^2 \begin{pmatrix} (1+\mu)q_2 + 4p_0p_1q_1 \\ -\beta q_2 - 4p_1^2 - 4p_2 - 2(p_1^2 + q_1^2)p_0 \end{pmatrix} + O(\epsilon^3).$$

The leading order outer dynamics reduces to a family of uncoupled ODEs,

$$\partial_{\tau} \begin{pmatrix} p_1 \\ q_1 \end{pmatrix} = \begin{pmatrix} (1+\mu)q_1 \\ -\beta q_1 - 4p_1 \end{pmatrix},$$

that induce exponential decay on the fast  $\tau = O(1)$  timescale. Setting  $u_1 = 0$  yields an equivalent system for  $u_2$ . We assume that  $u_1$  and higher order outer terms are zero on the relevant time scales. Correspondingly all matching of the inner system for  $i \ge 1$  is to the outer value 0.

# 3.2 Inner Expansion

The inner expansion uses the Frenet coordinates, for which in  $\mathbb{R}^n$  the scaled Laplacian takes the form

$$\epsilon^2 \Delta = \partial_z^2 + \epsilon \kappa_0(s) \partial_z + \epsilon^2 (z \kappa_1(s) \partial_z + \Delta_s) + \epsilon^3 (\Delta_{s,1} + z^2 \kappa_2(s) \partial_z) + O(\epsilon^4).$$

Here  $\Delta_s$  is the Laplace-Beltrami operator on the interface  $\Gamma$  and  $\kappa_0 = \sum_{j=1}^{n-1} k_j$  is the total curvature expressed in terms of the n-1 curvatures  $\{k_1, \ldots, k_{n-1}\}$  of  $\Gamma$ . The higher order curvatures satisfy

$$\kappa_i = (-1)^i \sum_{j=1}^{n-1} k_j^i,$$

for  $i \ge 1$  see Hayrapetyan and Promislow (2015, [eqn (6.37)]) and Dai and Promislow (2013, [eqn (2.8)]) for details. In two space dimensions, with n = 2, these relations



reduce to  $\kappa_i = (-1)^i \kappa_0^i$ . The inner expansion of the vector field residual

$$\tilde{F}(\tilde{U}) = \tilde{F}_0 + \epsilon \tilde{F}_1 + \epsilon^2 \tilde{F}_2 + \epsilon^3 \tilde{F}_3 + O(\epsilon^4), \tag{29}$$

requires an expansion of  $\tilde{U}$ ,

$$\tilde{U} = \tilde{U}_0 + \epsilon \tilde{U}_1 + \epsilon^2 \tilde{U}_2 + O(\epsilon^3),$$

where

$$\tilde{U}_0 = \begin{pmatrix} \phi \\ 0 \end{pmatrix}.$$

Since the higher order outer expansion is uniformly zero, the matching conditions to the outer solution devolve into requiring that each  $\tilde{U}_i(s,\cdot) \in L^2(\mathbb{R})$  for all values of s and all i > 1. The leading order residual has the form

$$\tilde{F}_0 = \begin{pmatrix} 0\\ \tilde{E}_0 \phi \end{pmatrix} = 0, \tag{30}$$

where we have introduced the operator

$$\tilde{\mathrm{E}}_0 := \partial_z^3 - 2\phi^2 + 2.$$

This leading order residual is zero since  $\phi$  solves (6) which is equivalent to  $\tilde{E}_0 \phi = 0$ . For  $i \ge 1$  the inner vector field residuals take the upper-triangular form

$$\tilde{F}_i = L\tilde{U}_i + \tilde{R}_i, \tag{31}$$

where L is given in (8). The lower order residuals  $\tilde{R}_i$  depend only upon  $\tilde{U}_k$  for  $k = 0, \ldots i - 1$ , and are given by

$$\tilde{R}_1 = \begin{pmatrix} 0 \\ \kappa_0 \partial_z \tilde{p}_0 \end{pmatrix},\tag{32}$$

$$\tilde{R}_2 = \begin{pmatrix} -\tilde{E}_1 \tilde{q}_1 \\ \tilde{E}_2 \tilde{p}_0 + \tilde{E}_1 \tilde{p}_1 \end{pmatrix}, \tag{33}$$

and

$$\tilde{R}_3 = \begin{pmatrix} -\tilde{E}_1 \tilde{q}_2 - \tilde{E}_2 \tilde{q}_1 \\ \tilde{E}_1 \tilde{p}_2 + \tilde{E}_2 \tilde{p}_1 + \tilde{E}_3 \tilde{p}_0 \end{pmatrix}, \tag{34}$$

where

$$\begin{split} \tilde{\mathbf{E}}_1 &= \kappa_0 \partial_z - 4 \tilde{p}_0 \tilde{p}_1, \\ \tilde{\mathbf{E}}_2 &= z \kappa_1 \partial_z + \Delta_s - 2 |\tilde{U}_1|^2, \\ \tilde{\mathbf{E}}_3 &= \Delta_{s,1} + z^2 \kappa_2(s) \partial_z - 4 \tilde{U}_1 \cdot \tilde{U}_2. \end{split}$$



To extract the curvature dynamics we develop a quasi-steady manifold U parameterized by the interface  $\Gamma$  through the scaled distance function z and the curvature  $\kappa_0$ . These quantities evolve on the slow time  $T=\epsilon^2\tau$  for which  $\epsilon^2\partial_T=\partial_\tau$ . The chain rule gives

$$D_T \tilde{U} = \frac{\partial \tilde{U}}{\partial z} \frac{\partial z}{\partial T} + \frac{\partial \tilde{U}}{\partial T}.$$
 (35)

The normal velocity V of the curve is scaled as  $V:=-\epsilon^{-1}\frac{\partial z}{\partial T}$ . This affords the reduction

$$\partial_{\tau}\tilde{U} = \epsilon^{2} D_{T}\tilde{U} = -\epsilon V \frac{\partial \tilde{U}}{\partial \tau} + \epsilon^{2} \frac{\partial \tilde{U}}{\partial T}.$$
 (36)

This is further expanded in terms of the normal velocity

$$V = V_0 + \epsilon V_1 + \epsilon^2 V_2 + O(\epsilon^3),$$

and the T partials of  $\tilde{U}$ ,

$$\partial_T \tilde{U} = \epsilon \partial_T \tilde{U}_1 + \epsilon^2 \partial_T \tilde{U}_2 + O(\epsilon^3),$$

for which  $\partial_T \tilde{U}_0 = 0$ . Combining these expansions yields the inner expansion of the left-hand side of (4),

$$\partial_{\tau}\tilde{U} = -\epsilon V_0 \partial_z \tilde{U}_0 - \epsilon^2 (V_0 \partial_z \tilde{U}_1 + V_1 \partial_z \tilde{U}_0) - \epsilon^3 (V_0 \partial_z \tilde{U}_2 + V_1 \partial_z \tilde{U}_1 + V_2 \partial_z \tilde{U}_0 - \partial_T \tilde{U}_1) + O(\epsilon^4)$$
(37)

Using (37) and (31) in (29) we match the  $O(\epsilon)$  terms in (4). This yields the system

$$-\begin{pmatrix} V_0 \\ \kappa_0 \end{pmatrix} \phi' = L\tilde{U}_1. \tag{38}$$

This is an elliptic problem in z for the leading order normal velocity  $V_0 = V_0(s)$  and  $\tilde{U}_1$ . The linear operator L has a kernel, so Fredholm's solvability condition requires

$$\begin{pmatrix} V_0 \\ \kappa_0 \end{pmatrix} \phi' \perp \Psi_0^{\dagger} = \begin{pmatrix} \beta D^{-1} \phi' \\ \phi' \end{pmatrix}.$$

This holds if the leading order normal velocity satisfies

$$V = -\alpha \kappa_0, \tag{39}$$

where the curvature coefficient  $\alpha = \alpha(\mu) \in \mathbb{R}$  satisfies

$$\alpha := \frac{\|\phi'\|^2}{\beta \langle D^{-1}\phi', \phi' \rangle}.$$
 (40)

40 Page 12 of 20 Journal of Nonlinear Science (2024) 34:40

This coefficient satisfies  $\alpha > 0$  so long as  $\mu > 0$ , corresponding to motion by curvature. It is instructive to expand  $\alpha$  in powers of  $\mu$ . From the relation (24) we find

$$\alpha = \mu \frac{\|\phi'\|^3 \|\psi\|}{\beta \langle \phi', \psi \rangle^2} + O(\mu^2). \tag{41}$$

We deduce that  $\alpha < 0$  for  $\mu$  small and negative, which implies an ill-posed motion against curvature. In the sequel we establish that the flow is regularized by higher order terms in the normal velocity expansion.

# 3.3 Regularization of the Normal Velocity

The first step to identify higher order terms in the normal velocity is to solve the system (38) for  $\tilde{U}_1$ . The inversion formula (16) applies if  $\mu \neq 0$ , and the system can be solved directly if  $\mu = 0$ . In either case the correction terms have a tensor-product structure

$$\tilde{U}_1(s,z) = \kappa_0(s)\overline{U}_1(z) = \kappa_0\left(\frac{\overline{p}_1}{\overline{q}_1}\right),$$
 (42)

in terms of s-dependent curvature and z-dependent vector-valued function  $\overline{U}_1$  which satisfies

$$\overline{U}_{1} = \begin{pmatrix} \mathbf{C}^{-1} \left( 1 - \beta \alpha \mathbf{D}^{-1} \right) \phi' \\ \alpha \mathbf{D}^{-1} \phi' \end{pmatrix} = \alpha \begin{pmatrix} -\beta \mathbf{C}^{-1} \Pi_{\phi'}^{\perp} \mathbf{D}^{-1} \phi' \\ \mathbf{D}^{-1} \phi' \end{pmatrix}, \quad \mu \neq 0, 
\overline{U}_{1} = \begin{pmatrix} \mathbf{C}^{-1} \left( \phi' - \frac{\|\phi'\|^{2}}{\langle \phi', \psi \rangle} \right) \\ \frac{\|\phi'\|^{2}}{\beta \langle \phi', \psi \rangle} \psi \end{pmatrix} = \frac{\|\phi'\|^{2}}{\beta \langle \phi', \psi \rangle} \begin{pmatrix} -\beta \mathbf{C}^{-1} \Pi_{\phi'}^{\perp} \psi \\ \psi \end{pmatrix}, \quad \mu = 0.$$
(43)

Here we have introduced the  $L^2(\mathbb{R})$  orthogonal projection

$$\Pi_{\phi'}^{\perp} f := f - \frac{\langle f, \phi' \rangle}{\|f\| \|\phi'\|} \phi', \tag{44}$$

which maps onto the orthogonal complement of the kernel of C. The formulas are smooth since

$$\alpha \mathrm{D}^{-1} \phi' \to \frac{\|\phi'\|^2}{\beta \langle \phi', \psi \rangle} \psi,$$

as  $\mu \to 0$ . In particular the function  $\overline{U}_1$  is uniformly bounded as  $\mu \to 0$  and has even parity in z. Returning to (4), we use (37) and (29) at  $O(\epsilon^2)$ . The form (33) yields the balance

$$L\tilde{U}_2 = -\tilde{R}_2 - (V_0 \partial_z \tilde{U}_1 + V_1 \partial_z \tilde{U}_0) = \begin{pmatrix} \tilde{E}_1 \tilde{q}_1 - V_0 \partial_z \tilde{p}_1 - V_1 \partial_z \tilde{p}_0 \\ -\tilde{E}_1 \tilde{p}_1 - \tilde{E}_2 \tilde{p}_0 - V_0 \partial_z \tilde{q}_1 \end{pmatrix}. \tag{45}$$



The solvabilty condition for  $\tilde{U}_2$  is the same as for  $\tilde{U}_1$ , however all the terms on the right-hand side of (45) have odd parity about z = 0 except for  $\partial_z \tilde{p}_0$ . This implies that the system is solvable for  $V_1 = 0$ . In two space dimensions  $\kappa_1 = -\kappa_0^2$  so that  $\tilde{E}_2$ can be written in terms of  $\kappa_0^2$ . Consequently the system for  $\tilde{U}_2$  has the tensor-product formulation

$$L\tilde{U}_2 = \begin{pmatrix} \omega_1 \\ \omega_2 \end{pmatrix} = \kappa_0^2 \begin{pmatrix} \overline{\omega}_1 \\ \overline{\omega}_2 \end{pmatrix},$$

where we have introduced

$$\overline{\omega}_1 := \partial_{z}(\overline{q}_1 + \alpha \overline{p}_1) - 4\phi \overline{p}_1 \overline{q}_1, \tag{46}$$

and

$$\overline{\omega}_2 := \partial_z (\alpha \overline{q}_1 - \overline{p}_1) + 4\phi \overline{p}_1^2 + 2|\tilde{U}_1|^2 \phi + z\phi'.$$

The functions  $\omega_1$  and  $\omega_2$  have odd parity about z=0, in particular  $D^{-1}\overline{\omega}_1$  is well defined and uniformly bounded as  $\mu \to 0$ . Inverting L we determine that

$$\begin{pmatrix} \tilde{p}_2 \\ \tilde{q}_2 \end{pmatrix} = \kappa_0^2 \begin{pmatrix} -C^{-1}(\beta D^{-1}\overline{\omega}_1 + \overline{\omega}_2) \\ D^{-1}\overline{\omega}_1 \end{pmatrix}. \tag{47}$$

This allows us to write

$$\tilde{U}_2 = \begin{pmatrix} \tilde{p}_2 \\ \tilde{q}_2 \end{pmatrix} = \kappa_0^2(s) \begin{pmatrix} \overline{p}_2(z) \\ \overline{q}_2(z) \end{pmatrix} = \kappa_0^2 \overline{U}_2,$$

where  $\overline{U}_2$  has odd parity in z. To determine  $V_2$  we proceed to the  $O(\epsilon^3)$  matching in the inner expansion of (4). Equating (34) with the  $O(\epsilon^3)$  terms in (37) yields

$$\begin{pmatrix} -V_0 \partial_z \tilde{p}_2 - V_2 \partial_z \tilde{p}_0 \\ -V_0 \partial_z \tilde{q}_2 \end{pmatrix} + \partial_T \kappa_0 \overline{U}_1 = L \tilde{U}_3 + \tilde{R}_3.$$

The solvability conditions require that the terms without  $\tilde{U}_3$  are orthogonal to  $\Psi_0^{\dagger}$ , which has even parity about z = 0. This yields the system

$$\begin{pmatrix} -V_0 \partial_z \tilde{p}_2 - V_2 \phi' + \partial_T \kappa_0 \overline{p}_1 + \tilde{E}_1 \tilde{q}_2 + \tilde{E}_2 \tilde{q}_1 \\ -V_0 \partial_z \tilde{q}_2 + \partial_T \kappa_0 \overline{q}_1 - \tilde{E}_1 \tilde{p}_2 - \tilde{E}_2 \tilde{p}_1 - \tilde{E}_3 \tilde{p}_0 \end{pmatrix} \perp \Psi_0^{\dagger}, \tag{48}$$

to be solved for  $V_2$ . From, Pismen (2006) in two space dimensions the co-moving coordinates imply the relation between normal velocity and evolution of the curvature,

$$\partial_T \kappa_0 = -(\Delta_s + \kappa_0^2) V = \alpha (\Delta_s \kappa_0 + \kappa_0^3) + O(\epsilon^2). \tag{49}$$

40 Page 14 of 20 Journal of Nonlinear Science (2024) 34:40

This allows the left-hand side of (48) to be expressed as a tensor product of  $\Delta_s \kappa_0$  and  $\kappa_0^3$  and vector valued functions  $\overline{W}_1$  and  $\overline{W}_2$  of z-only dependence,

$$\left(\Delta_s \kappa_0 \overline{W}_1 + \kappa_0^3 \overline{W}_2 - V_2 \partial_z \overline{U}_0\right) \bot \Psi_0^{\dagger}.$$

These *z*-only vector-valued functions take the form

$$\overline{W}_1 = \begin{pmatrix} \alpha \overline{p}_1 + \overline{q}_1 \\ -\overline{p}_1 + \alpha \overline{q}_1 \end{pmatrix}, \tag{50}$$

and

$$\overline{W}_{2} = \begin{pmatrix} \alpha \left( \partial_{z} \overline{p}_{2} + \overline{p}_{1} \right) + \partial_{z} \overline{q}_{2} - 4\phi \overline{p}_{1} \overline{q}_{2} - z \partial_{z} \overline{q}_{1} - 2 |\overline{U}_{1}|^{2} \overline{q}_{1} \\ \alpha \left( \partial_{z} \overline{q}_{2} + \overline{q}_{1} \right) - \partial_{z} \overline{p}_{2} + 4\phi \overline{p}_{1} \overline{p}_{2} + z \partial_{z} \overline{p}_{1} + 2 |\overline{U}_{1}|^{2} \overline{p}_{1} - z \phi' + 4 \overline{U}_{1} \cdot \overline{U}_{2} \phi \end{pmatrix}.$$

$$(51)$$

Solving for  $V_2$  yields the higher order corrections to the normal velocity,

$$V_2 = \nu \Delta_s \kappa_0 + \zeta \kappa_0^3. \tag{52}$$

where the coefficients are defined by

$$\nu := \frac{\langle \overline{W}_1, \Psi_0^{\dagger} \rangle}{\beta \langle D^{-1} \phi', \phi' \rangle},\tag{53}$$

and

$$\zeta := \frac{\langle \overline{W}_2, \Psi_0^{\dagger} \rangle}{\beta \langle D^{-1} \phi', \phi' \rangle}.$$
 (54)

Parity considerations imply that  $V_3 = 0$  as they did for  $V_1$ , and hence the normal velocity has no  $O(\epsilon^3)$  terms and

$$V = -\alpha \kappa_0 + \epsilon^2 \left( \nu \Delta_s \kappa_0 + \zeta \kappa_0^3 \right) + O(\epsilon^4). \tag{55}$$

Moreover the  $O(\epsilon^4)$  terms are bounded relative to  $1 - \Delta_s$  and hence reflect regular perturbations.

The sign of  $\nu$  is essential to the wellposedness of the normal velocity system. In particular wellposedness requires  $\nu > 0$ . Applying the formula for the adjoint kernel  $\Psi_0^{\dagger}$ , (15), to (53) yields,

$$\nu = \frac{\langle \alpha \overline{p}_1 + \overline{q}_1, \beta D^{-1} \phi' \rangle + \langle -\overline{p}_1 + \alpha \overline{q}_1, \phi' \rangle}{\beta \langle D^{-1} \phi', \phi' \rangle},$$
 (56)



however  $\overline{p}_1 \perp \phi'$  so their inner product is zero. Using (43) to expand  $\overline{U}_1$  we find

$$\nu = -\frac{\|\phi'\|^4 \beta \langle \mathbf{C}^{-1} \Pi_{\phi'}^{\perp} \mathbf{D}^{-1} \phi', \Pi_{\phi'}^{\perp} \mathbf{D}^{-1} \phi' \rangle}{\langle \mathbf{D}^{-1} \phi', \phi' \rangle^3} + \frac{\|\phi'\|^2 \|\mathbf{D}^{-1} \phi'\|^2}{\beta \langle \mathbf{D}^{-1} \phi', \phi' \rangle^2} + \frac{\|\phi'\|^4}{\beta^3 \langle \mathbf{D}^{-1} \phi', \phi' \rangle^2}.$$
(57)

For  $|\mu|$  small the asymptotic inverse formula

$$D^{-1}\phi' = \frac{\langle \phi', \psi \rangle}{\|\phi'\| \|\psi\|} \frac{\psi}{\mu} + O(1), \tag{58}$$

shows that the second term in (57) is dominant for small  $\mu$ ,

$$\nu = \frac{\|\phi'\|^2 \|\psi\|^2}{\langle \psi, \phi' \rangle^2} + O(\mu)$$
 (59)

which is positive for  $|\mu| < \mu_*$ , for  $\mu_* > 0$  sufficiently small, independent of  $\epsilon$ . This establishes the main result (1).

Assuming that the curvatures are bounded uniformly with respect to  $\epsilon$ , the  $\epsilon^2 \zeta \kappa_0^3$  term in (55) is asymptotically small compared to  $\alpha \kappa_0$  unless  $\zeta$  is bounded away from zero and  $\alpha = O(\epsilon^2)$ . This occurs when  $\mu = O(\epsilon^2)$ . Since  $\zeta = \zeta(\mu)$  is smooth in  $\mu$  it remains to approximate  $\zeta(0)$ . The terms  $\overline{U}_1$  and  $\overline{U}_2$  are smooth in  $\mu$  and in particular are bounded as  $\mu \to 0$ . The denominator of  $\zeta$  scales like  $\mu^{-1}$  as  $\mu \to 0$  so only the terms  $\langle \overline{W}_{21}, \beta D^{-1} \phi' \rangle$  can give a nonzero contribution to  $\zeta(0)$ . That is, for  $|\mu| \ll 1$  the inverse formula (58) yields

$$\zeta = \frac{\langle \overline{W}_{21}, D^{-1} \phi' \rangle}{\langle D^{-1} \phi', \phi' \rangle} + O(\mu) = \frac{\langle \overline{W}_{21}, \psi \rangle}{\langle \psi, \phi' \rangle} + O(\mu).$$

Since  $\alpha \to 0$  smoothly as  $\mu \to 0$  terms in  $\overline{W}_{21}$  containing  $\alpha$  are also  $O(\mu)$ . We introduce the z-only reductions of the operators  $\tilde{E}_1$  and  $\tilde{E}_2$ ,

$$\overline{\mathbf{E}}_1 := \partial_z - 4\phi \overline{p}_1, 
\overline{\mathbf{E}}_2 := z\partial_z - 2|\overline{U}_1|^2,$$

and observe that (46) can be written as  $\overline{\omega}_1 = \overline{E}_1 \overline{q}_1 + O(\mu)$ . This allows  $\overline{W}_{21}$  to be expanded in the symmetric form

$$\overline{W}_{21} = \frac{\|\phi'\|^2}{\langle \phi', \psi \rangle} \left( \overline{\mathbf{E}}_1 \mathbf{D}^{-1} \overline{\mathbf{E}}_1 + \overline{\mathbf{E}}_2 \right) \psi + O(\mu),$$



and hence

$$\begin{split} \zeta &= \frac{\|\phi'\|^2}{\langle \phi', \psi \rangle^2} \left( \langle D^{-1} \overline{\mathbf{E}}_1 \psi, \overline{\mathbf{E}}_1^{\dagger} \psi \rangle + \langle \overline{\mathbf{E}}_2 \psi, \psi \rangle \right) + O(\mu), \\ &= \frac{\|\phi'\|^2}{\langle \phi', \psi \rangle^2} \left( -\langle D^{-1} \psi', \psi' \rangle + 16 \langle D^{-1} (\phi \overline{p}_1 \psi), \phi \overline{p}_1 \psi \rangle - \frac{1}{2} \|\psi\|^2 - 2 \langle |\overline{U}_1|^2, \psi^2 \rangle \right) \\ &+ O(\mu). \end{split}$$

The coefficient  $\zeta$  at  $\mu=0$ , is a sum of three negative and one positive term, and hence is sign indefinite.

## 4 Numerical Confirmation and Discussion

The length of a closed interface  $\Gamma$  evolving under a normal velocity V satisfies

$$\partial_T |\Gamma| = \int_{\Gamma} V \kappa_0 \, ds. \tag{60}$$

For the system (55) following an integration by parts this reduces to

$$\partial_T |\Gamma| = -\int_{\Gamma} \left( \alpha |\kappa_0|^2 + \epsilon^2 \nu |\nabla_s \kappa_0|^2 - \epsilon^2 \zeta |\kappa_0|^4 \right) ds + O(\epsilon^4). \tag{61}$$

If the curvature is uniformly bounded by M>0, then the interfacial length decreases if  $\alpha>\epsilon^2\zeta M^2$ . In particular a circular interface  $\Gamma$  with an O(1) radius  $R=R_*$  is an equilibrium if and only if  $\alpha,\zeta>0,\alpha=O(\epsilon^2)$  and

$$R_* = \epsilon \sqrt{\frac{\zeta}{\alpha}}. (62)$$

Conversely if  $\alpha < 0$  is O(1) and the curvature is not zero, then the length of a smooth interface will grow. From (49) the normal velocity induces the complicated evolution equation

$$\partial_T \kappa_0 = (\Delta_s + \kappa_0^2)(\alpha \kappa_0 - \nu \epsilon^2 \Delta_s \kappa_0 - \epsilon^2 \zeta \kappa_0^3) + O(\epsilon^4),$$

in which surface diffusion acts as a singular perturbation. Generically a simple closed interface will grow, buckle (meander), and self-intersect.

These results are supported by simulations of (2) shown in Fig. 2. The modulus  $|\Theta|$  of the solution  $\Theta$  of the PNLS system is zero on the interface and tends to an identical constant value in both  $\Omega_{\pm}$  domains. Each simulation starts with the same initial data,

$$\Theta_0(x) = A \tanh((|x| - r(\theta))/\epsilon),$$



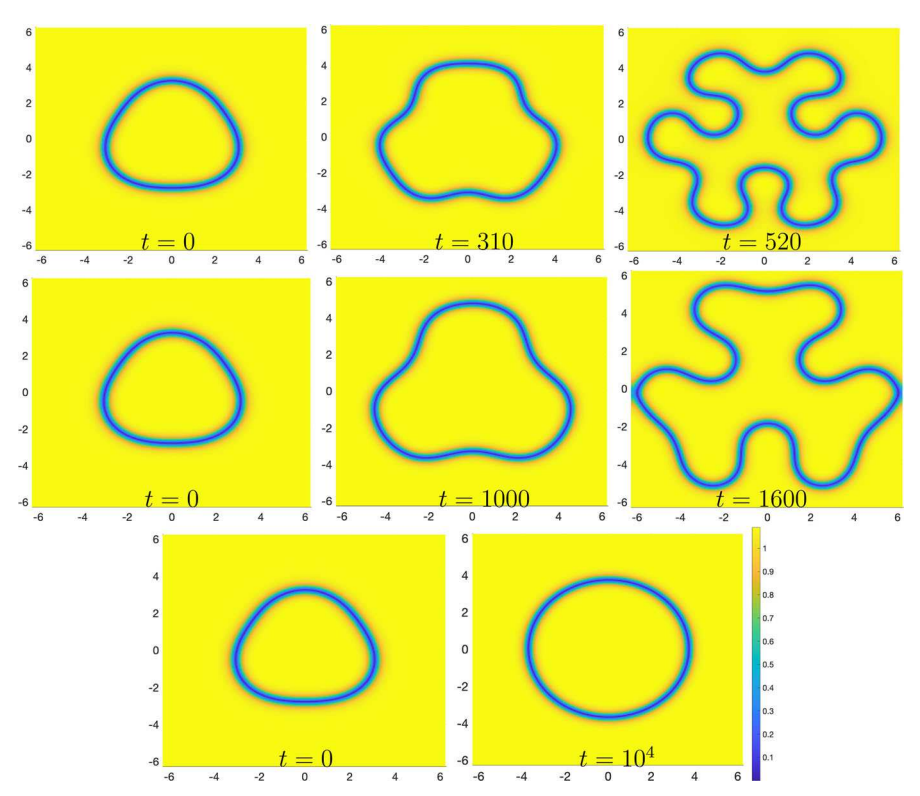


Fig. 2 Contour plots of the modulus  $|\Theta|$  over  $[-2\pi, 2\pi]^2$  simulated from (2) for (top row)  $\mu = -0.503$  and  $\beta = 3.50$ , (middle row)  $\mu = -0.208$  and  $\beta = 3.21$ , (bottom row)  $\mu = 0.0405$  and  $\beta = 2.96$ . In all simulations  $\epsilon = 0.3$  and unscaled time t is as indicated, with common color bar indicated in last row (Color figure online)

where  $A \in \mathbb{C}$  is the complex equilibrium of (2),  $\theta$  is the angle x makes to the  $x_1$ -axis, and

$$r(\theta) = 3 + \frac{1}{10} \left( \sin(3\theta) - \sin^2(7\theta) \right),$$

is a closed perturbation of a circular interface of radius 3. The function  $|\Theta_0|$  is depicted in the left-most image in each row of Fig. 1. The dispersive ratio  $\epsilon=0.3$  in all simulations and the periodic domain  $\Omega=[-2\pi,2\pi]^2$  is discretized using  $256^2$  Fourier modes. The top row shows the results for  $\mu=-0.503$  and  $\beta=3.50$  which is well into the motion against curvature regime. The interface lengthens and buckles, and self-intersects soon after the last t=520 time depicted. Subsequent evolution generates the complex motion of front-type cells discussed below. The second row depicts the simulations for  $\mu=-0.208$  and  $\beta=3.21$ . This has weaker motion against curvature, the maximum curvature attained is smaller and the interface growth just yielded self-intersected (across the periodic boundary) at t=1600, although the interface has filled the domain. The third row corresponds to  $\mu=0.0405$  which



40 Page 18 of 20 Journal of Nonlinear Science (2024) 34:40

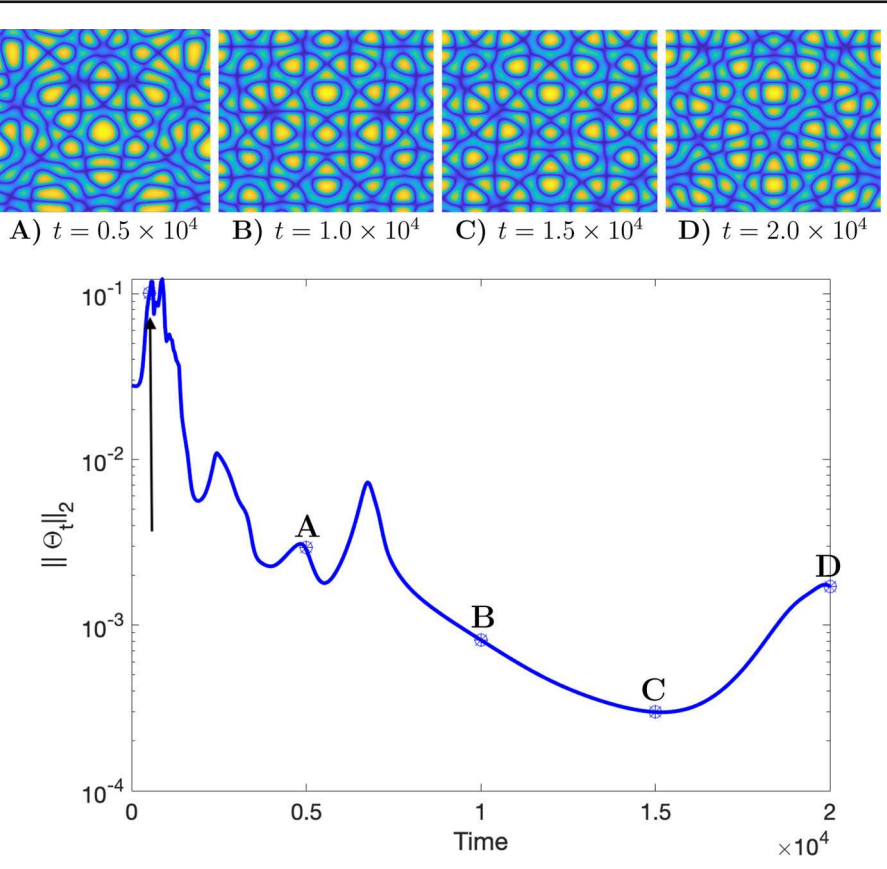


Fig. 3 (Top) Contour plots of the modulus  $|\Theta|$  over  $[-2\pi, 2\pi]^2$  simulated from Eq. (2) for  $\mu=-0.503$ ,  $\beta=3.50$ , and  $\epsilon=0.3$  at times  $\mathbf{A}\ t=5000$ ,  $\mathbf{B}\ T=10,000$ ,  $\mathbf{C}\ t=15,000$ , and  $\mathbf{D}\ t=20,000$ . The simulation used the same initial data and color bar as those presented in Fig. 2. (Bottom) Semi-log plot of  $\|\Theta_t\|_2$  verses time. The labeled points A–B–C–D corresponding to the snapshots of the top row and the vertical arrow indicates the last frame of the top row of Fig. 2 roughly corresponding to the time of first intersection of the interface

is positive but smaller than  $\epsilon^2=0.09$ . This is in the curvature-driven flow regime, and the interface evolves into a circle with limiting radius R=3.75. The computed values  $\zeta=0.576$  and  $\alpha=0.0121$  yield the equilibrium radius  $R_*=3.78$ , showing good quantitative agreement between the asymptotic reduction and the numerical simulation. Computations with positive  $\mu=0.159$  and  $\beta=2.84$  (not shown) yield a circular interface that shrinks and approaches an  $O(\epsilon)$  radius where it remains until t=3000 at which time the interface collapses and the function  $\Theta$  becomes spatially constant. Circular interfaces of  $O(\epsilon)$  radius are near self-intersection and their analysis is outside the scope of this work.

Continuation of the flow subsequent to self-intersection brings the evolution out of the regime of the front dynamics analyzed above. However we include simulations in this regime to illustrate the impact of motion against curvature on system complexity. For  $\mu < 0$ , numerical simulations beyond front self-intersection show that the flow



enters a regime dominated by cells that exhibit a complex jostling motion. Extending the flow depicted in the top row of Fig. 2 corresponding to  $\mu=-0.503$ , to times beyond the front self-intersection shows that front breaks into cells of positive or negative phase demarcated by lines of zero intensity ( $|\Theta|=0$ ). These cells experience a strong jostling up to a time of order t=5000, and then settle into a regime of slower but unsteady motion for times on the order  $t\in[10^4,2\times10^4]$ . Snapshots of the modulus  $|\Theta|$  at times A)  $t=0.5\times10^4$ , B)  $t=1.0\times10^4$ , C)  $t=1.5\times10^4$  and D)  $t=2.0\times10^4$  are depicted in the top row of Fig. 3. The slight differences between snapshots B and C (principally at the bottom of the two frames) might suggest convergence to equilibrium. However the considerable differences between snapshot C and D suggest that the configuration in C is a quasi-equilibrium or saddle point of the flow.

The structure within the flow is better revealed by examining the time evolution of the  $L^2$  norm of the time derivative of  $\Theta$ :  $\|\Theta_t\|_2$ . As shown in Fig. 3 (bottom), the norm initially increases during the time period prior to the first self-intersection, t=520, marked by the vertical arrow. Subsequently the flow remains dominated by motion against curvature until roughly t<1000. During this period the time derivative scales like  $\|\Theta_t\|_2\approx 10^{-1}$ . The flow transitions to an active 'jostling of cells' motion for  $t\in(0.2\times10^4,0.8\times10^4)$  for which  $\|\Theta_t\|_2\approx 10^{-2}$ . This regime is represented by snapshot A in the top row of Fig. 3. On the longer time frame,  $t>0.8\times10^4$ , the evolution appears to relax, with  $\|\Theta_t\|_2$  decreasing below  $10^{-3}$ . This slow evolution generates the relative similarity of snapshots B and C. However the subsequent excursion brings  $\|\Theta_t\|_2$  back above  $10^{-3}$  and generates the significant differences in the later configuration represented by snapshot D.

The analysis presented is the first to capture the transition from motion with curvature to motion against curvature in a dispersive system. The analysis is formal, but is qualitatively accurate in the regime in which  $|\mu|$  is sufficiently small. This is verified by the accurate prediction of the limiting equilibrium radius  $R_*$  as simulated numerically in the case  $\mu=0.0405$  in Fig. 2 (bottom row). This work examines the role of bifurcations in front dynamics that initiate interfacial growth as a broader trigger for the development of complexity in forced-damped systems. We feel that the generality of this mechanism merits further study.

**Acknowledgements** The first author acknowledges NSF support through grant DMS 2205553.

#### References

Alexander, J.C., Grillakis, M.G., Jones, C.K.R.T., Sandstede, B.: Stability of pulses on optical fibers with phase-sensitive amplifiers. Zeitshcrift für angewandte Mathematik und Physik (ZAMP) 48, 175–192 (1997)

Chen, Y., Promislow, K.: Curve lengthening via regularized motion against curvature from the strong FCH gradient flow. J. Dyn. Differ. Equ. 25, 1785–1841 (2023). https://doi.org/10.1007/s10884-022-10178-7

Coulibaly, S., Durniak, C., Taki, M.: Spatial dissipative solitons under convective and absolute instabilities in optical parametric oscillators. In: Dissipative Solitons: From Optics to Biology and Medicine edited by A. Ankiewicz and N. Akhmediev, Lecture Notes Physics, vol. 751, pp. 261–287 (2008)



40 Page 20 of 20 Journal of Nonlinear Science (2024) 34:40

Coulibaly, S., Taki, M., Tlidi, M.: Universal power law for front propagation in all fiber resonators. Opt. Express 22, 483–489 (2014)

- Dai, S., Promislow, K.: Geometric evolution of bilayers under the functionalized Cahn–Hilliard equation. Proc. R. Soc. 469, 20120505 (2013)
- Hayrapetyan, G., Promislow, K.: Spectra of functionalized operators arising from hypersurfaces. Zeitschrift für angewandte Mathematik und Physik (ZAMP) 66, 631–662 (2015)
- Izús, G., Santagiustina, M., San Miguel, M., Colet, P.: Pattern formation in the presence of walk-off for a type II optical parametric oscillator. J. Opt. Soc. Am. B 16, 1592–1596 (1999)
- Kapitula, T., Promislow, K.: Stability indices for constrained self-adjoint operators. Proc. Am. Math. Soc. 140(3), 865–88 (2012)
- Kapitula, T., Promislow, K.: Spectral and Dynamical Stability of Nonlinear Waves. Applied Mathematical Sciences. Springer, New York (2013)
- Pismen, L.M.: Patterns and Interfaces in Dissipative Dynamics. Springer Series in Synergetics. Springer, Berlin (2006)
- Promislow, K., Kutz, J.N.: Bifurcation and asymptotic stability in the large detuning limit of the optical parametric oscillator. Nonlinearity 13, 675–698 (2000)
- Ropp, C., Bachelard, N., Barth, D., Wang, Y., Zhang, X.: Dissipative self-organization in optical space. Nat. Photon 12, 739–743 (2018)
- Roy, A., Jahani, S., Langrock, C., Fejer, M., Marandi, A.: Spectral phase transitions in optical parametric oscillators. Nat. Commun. 12(1), 835 (2021)
- Taki, Majid, Ouarzazi, Najib, Ward, Hélène., Glorieux, Pierre: Nonlinear front propagation in optical parametric oscillators. J. Opt. Soc. Am. B 17, 997–1003 (2000)
- Trillo, S., Haelterman, M., Sheppard, A.: Stable topological spatial solitons in optical parametric oscillators. Opt. Lett. 22(13), 970–972 (1997)
- Zhang, W., Viñals, J.: Secondary instabilities and spatiotemporal chaos in parametric surface waves. Phys. Rev. Lett. 74, 690 (1995)

Publisher's Note Springer Nature remains neutral with regard to jurisdictional claims in published maps and institutional affiliations.

Springer Nature or its licensor (e.g. a society or other partner) holds exclusive rights to this article under a publishing agreement with the author(s) or other rightsholder(s); author self-archiving of the accepted manuscript version of this article is solely governed by the terms of such publishing agreement and applicable law.

